Buckling transition in icosahedral shells subjected to volume conservation constraint and pressure: Relations to virus maturation

Antonio Šiber*
Institute of Physics, P.O. Box 304, 10001 Zagreb, Croatia
(Received 3 February 2006; revised manuscript received 6 April 2006; published 21 June 2006)

Minimal energy shapes of closed, elastic shells with 12 pentagonal disclinations introduced in otherwise hexagonally coordinated crystalline lattice are studied. The geometry and the total energy of shells are studied as a function of the elastic properties of the material they are made of. Particular emphasis is put on the *buckling transition* of the shells, that is, a strong preference of the shell shapes to "buckle out" in spatial regions close to the pentagonal disclinations for a certain range of the elastic parameters of the problem. The transition effectively increases the mean square asphericity of shapes, making them look more like an icosahedron rather than a sphere, which is a preferred shape prior to the onset of the transition. The properties of the buckling transition are studied in cases when (i) the total volume enclosed by the elastic shell has to be fixed and when (ii) there is an internal pressure acting on the shell. This may be related to the maturation process in nonenveloped dsDNA viruses, where the insertion of the genetic material in a preformed protein shell (viral coating) may effectively impose the fixed volume and/or pressure constraint. Several scenarios that may explain the experimentally observed feature of mature viruses being more aspherical (facetted) from their immature precursors are discussed, and predictions for the elastic properties of viral coatings are obtained on the basis of the presented studies.

DOI: 10.1103/PhysRevE.73.061915 PACS number(s): 87.68.+z, 87.15.La, 46.32.+x, 68.60.Bs

I. INTRODUCTION

Several articles have appeared recently that aim to describe the virus structure, shape, and stability by using physical principles. Virus-related research seems to be particularly appealing to physicists since viruses exhibit many features that are reminiscent of well known and thoroughly studied phenomena in "more traditional" physical systems. For example, 50 years ago Fraenkel-Conrat demonstrated that infectious viral particles [tobacco mosaic viruses (TMV)] can be reassembled from two solutions, one containing the viral genetic material (RNA) and the other its coat (or *capsid*) proteins (a short historical overview of research on reconstitution of TMV can be found in Ref. [1]). The reassembly of TMV proceeds without any special external impetus—it is spontaneous. The fact that viruses can be reassembled in *in vitro* conditions suggests that their shape and symmetry should be a result of free energy minimization, a concept familiar from equilibrium thermodynamics. This line of thought has recently been successfully applied in the explanation of the physical *origin* of the icosahedral symmetry of viruses (see below) and other possible shapes and geometries that might be adopted by viruses [2,3]. The production of a functional molecular machine from its constituent, possibly engineered molecular components is a dream of nanotechnologists. Such an approach to "molecular engineering" does not require precise molecular positioning, since correct assembly takes place *spontaneously* due to specific architecture of the molecular constituents and pronounced anisotropy of their mutual interactions; hence, the term *self-assembly* is often used in a nanotechnological context.

The structural symmetry and shape of virus coating is in itself intriguing. There have been attempts to draw parallels between the symmetry of viruses, Penrose tilings [4], and quasicrystals [5]. Most viruses have a structure with topology equal to that of triangulated icosahedra (see Fig. 1). Individual proteins that make the viral coating (approximated by triangles in Fig. 1) are organized in units called *capsomers* that consist of five (pentamers) or six protein units (hexamers). Most viruses contain only 12 pentamers and remaining capsomers are hexamers [6]. Pentamers are located at 12 vertices of an icosahedron. Such structures are very similar to giant fullerene molecules [7]. It is also easy to see a structural relationship between the virus and an icosahedral geodesic dome [8]. One of the simplest virus structures ($T=3$, see below), characteristic of small viruses (e.g., cucumber mosaic virus [9]), contains 12 pentamers and 20 hexamers and is topologically equivalent to a famous buckminsterfullerene molecule (C_{60}) [10]. Icosahedral symmetry that is characteristic of viral shapes is also frequently found in ground state configurations of atomic clusters (see, e.g., Ref.

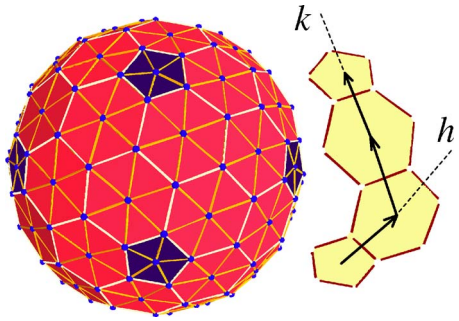

FIG. 1. (Color online) Idealized $T=7$ ($h=1$, $k=2$) virus structure. The structure consists of 12 pentamers (at the vertices of an icosahedron) and 60 hexamers. Note how the neighboring pentamers can be connected with two subsequent translations along two distinct spherical geodesics.

*Electronic address: asiber@ifs.hr

[11]). Poligonalizaton of a sphere with pentagons and hexagons is often described in terms of Caspar-Klug quasiequivalent construction [12]. Within this framework, viruses are characterized by the so-called *T number*, which describes the order of a poligonalization. The T number can be written as $T=h^2+k^2+hk$, where h and k are non-negative integers. The meaning of these integers can be quickly grasped from Fig. 1. Note how the two neighboring pentamers in the structure displayed in Fig. 1 can be connected through two subsequent translations along two distinct spherical geodesics. The magnitudes of these translations are non-negative integer multiples (h and k) of distances between the nearest-neighboring capsomers, so that the structure in Fig. 1 can be characterized by $h=1$ and $k=2$, or $T=7$. The total number of capsomeric units in a virus of particular T number symmetry is $10T+2$. Twelve of these units are pentamers and remaining $10(T-1)$ are hexamers [6].

The shapes of viral capsids have been recently studied within the framework of nonlinear theory of elastic shells [13,14]. These studies have produced rather interesting results, and excellent fits to experimentally determined virus shapes have been obtained [13]. The most important feature of the shell shapes that these studies predict is the *buckling transition*. The buckling transition has been earlier predicted for planar triangular meshes with a pentagonal or heptagonal defect introduced in their structure [15]. As a consequence of minimization of the total energy, which includes both stretching and bending contributions, the crystalline mesh buckles in a conical shape in the vicinity of a pentagonal defect (or disclination). This transition is observed only above the critical value of the so-called *Foppl–von Kármán number* (γ) [15], which is an effective parameter combining the mesh radius, two-dimensional Young's modulus (Y), and bending rigidity (κ). This parameter uniquely describes the shape of continuous shells. A pentagonal "defect" (pentamer) is characteristic of a virus structure, and viral coating can thus be viewed as a continuous shell with 12 pentagonal disclinations introduced in otherwise hexagonally coordinated crystalline structure (each vertex in the "regular" mesh has six nearest neighbors). The two studies [13,14] have reached the conclusion that the remnants of buckling transitions survive in the more complex geometry of a spherical (closed) shell with 12 pentagonal disclinations. This transition is not as sharp as in the case of a (two-dimensional) disk; nevertheless, an observable buckling transition of the shell was found for Föppl–von Kármán (FvK) numbers between about $\gamma=100$ and 1000. This effect has been related to the features of the experimentally determined virus shapes, and it can correctly describe the global trend of larger viruses being more faceted (or buckled) than smaller ones [16]. One of the interesting propositions put forth by the authors of Ref. [13] is that the process of virus maturation can be described in part by the buckling transition of viral capsids. Virus maturation is the process through which the assembled viral particles become fully functional. Its precise evolution depends on the type (or family) of the virus in question, in particular, whether the viruses are enveloped by the cell membrane proteins or not. For a large class of nonenveloped viruses [e.g., those containing the double stranded DNA (ds-DNA) in their mature form [16]], the maturation consists of incorporation of the genetic material in a preassembled, empty protein capsid (the so-called precursor capsid or *procapsid*). During the maturation process the capsid typically swells, and mature capsids are larger from their precursor counterparts. A faceted shape is often a characteristic of a mature virus, whereas (immature) precursor capsids have a more spherical shape. This transition in shape has been described within a framework of the elastic theory of shells in terms of the change of the FvK number [13]—the FvK number in mature viral shells is larger than in their respective precursor capsids. However, during the buckling transition of elastic shells, the volume enclosed by the shell *decreases*, whereas for most viruses, the mature viral capsids enclose *larger* volume from the immature precursor capsids [17,18].

The aim of this paper is to investigate whether the buckling transition in elastic shells survives in more restrictive circumstances, in particular, under the constraint of volume conservation and when the internal pressure acting on the shell is nonvanishing. These constraints may be thought of as the simplest possible introduction of the capsid-DNA/RNA interaction in the problem of virus shapes. Thus, an investigation of the characteristics of buckling transition in more general conditions should be of use for a more thorough understanding of viral capsid shapes in their immature and mature forms.

The paper is organized as follows. Section II briefly discusses the model of elasticity and minimal energy shapes of shells with 12 pentagonal disclinations subjected to a constraint of fixed volume. Section III contains the results pertaining to empty shells, i.e., without the imposition of the fixed enclosed volume or constant pressure constraints. This section deals with the subject already treated in Refs. [13,14], and its main purpose is to clearly demonstrate that the *shell volume decreases during the buckling transition*. In Sec. IV, the minimal energy shell shapes with the imposed constraint of fixed enclosed volume are studied. It is shown that the buckling transition survives in that case also, although the buckled shapes are less aspherical than the ones obtained without the volume conservation constraint. Section V contains results regarding the buckling transition of shells subjected to constant environmental pressure (the difference in pressures in the inner and outer space of the shell is fixed). Section VI relates the results of the article to the virus maturation process. Several possible scenarios that reproduce the experimentally observed fact of mature viruses being more aspherical and facetted as compared to their immature precursors are discussed. Predictions for the parameters characterizing the elastic response of viral coatings are given. Section VII briefly summarizes the results and concludes the paper.

II. A MODEL OF ELASTIC SHELLS WITH THE CONSTRAINTS OF FIXED ENCLOSED VOLUME AND CONSTANT PRESSURE

I start from the model of elasticity described in Refs. [13–15]. Briefly, the shell surface is discretized in triangular plaquettes and the Hamiltonian describing such a system is

$$H = \frac{\epsilon}{2}\sum_{i,j}(|\mathbf{r}_i - \mathbf{r}_j| - a)^2 + \frac{\tilde{\kappa}}{2}\sum_{I,J}(\mathbf{n}_I - \mathbf{n}_J)^2, \quad (1)$$

where indices i and j (I and J) describe the two neighboring triangle vertices (surfaces) located at $\mathbf{r}_i$ and $\mathbf{r}_j$, respectively, ϵ is the scale of energy related to a change of the distance between the two neighboring vertices (stretching), while $\tilde{\kappa}$ is the scale of energy related to a change of dihedral angle (bending) between the two neighboring triangles (those sharing a side) whose normal vectors are denoted by $\mathbf{n}$. The equilibrium distance between the two neighboring vertices is a, and it is assumed that the neighboring triangular plaquettes prefer to lie in the same plane, i.e., the preferred angle between their normal vectors is zero. The authors of Ref. [14] considered also the case of nonzero preferred curvature of the surface which can be simply introduced in the above Hamiltonian [14]. For surfaces containing a very large number of triangular plaquettes, the discrete Hamiltonian becomes reliable for the description of continuous elastic medium described by Young's modulus $Y=2\epsilon/\sqrt{3}$, Poisson's ratio $\nu=1/3$, bending rigidity $\kappa=\sqrt{3}\tilde{\kappa}/2$, and Gaussian rigidity $\kappa_G=-4/3$ [13].

Finding a minimum-energy state (or a shape) of a problem defined by Eq. (1) consists of a multidimensional search for a minimum of the Hamiltonian function $H(\mathbf{r}_1,\ldots,\mathbf{r}_N)$ that depends on $3N$ coordinates, where N is the number of mesh vertices. This search is unconstrained which means that there are no relationships between the variables $\mathbf{r}_1,\ldots,\mathbf{r}_N$ that have to be obeyed.

A. Enclosed volume constraint

It is possible to do a constrained search for the minimum of Eq. (1), specifying additionally some relations that the variables (or a shape) have to obey. The volume of a shell can be expressed in terms of the coordinates of the mesh vertices as

$$V = \frac{1}{6}\sum_I |\mathbf{r}_{I,1}\cdot(\mathbf{r}_{I,2}\times\mathbf{r}_{I,3})|, \quad (2)$$

where $\mathbf{r}_{I,1},\mathbf{r}_{I,2}$, and $\mathbf{r}_{I,3}$ are the three vertices of the triangle I in (counter)clockwise order. A search for a minimum of Eq. (1) with the independent variables (vertex coordinates) additionally fulfilling $V=V_0$, where V_0 is a fixed quantity, should result in a shape that minimizes the function $H(\mathbf{r}_1,\ldots,\mathbf{r}_N)$ in the subspace of all possible shapes that enclose volume V_0. The volume constraint is implemented in the numerical procedure using the so-called penalized version of the Hamiltonian [19], where an additional, quadratic penalty term of the form

$$H_V = \frac{\lambda}{2}(V - V_0)^2 \quad (3)$$

is added to the original Hamiltonian in Eq. (1), so that the new Hamiltonian (H_n) is given by $H_n=H+H_V$. Ideally, a penalty parameter λ should be extremely large (and positive) to strictly impose the volume constraint. The problem of finding a minimum of a strongly constrained Hamiltonian is solved using the so-called continuation technique [19]. A small value of λ is chosen initially, which enables a quick numerical convergence of the shape. This shape is used as an initial guess for the Hamiltonian in which λ is ten times larger ($\lambda\rightarrow 10\lambda$), and the procedure is repeated until λ is large enough so that the volume constraint is fulfilled to a machine precision.

B. Constant internal pressure

The constant internal pressure (p) is introduced in the problem by adding to the shell Hamiltonian a term pV, so that the new Hamiltonian of the problem (H_n) is given by

$$H_n = H + pV. \quad (4)$$

This introduces an additional force $\Delta\mathbf{F}_i$ on the ith vertex which is given by $\Delta\mathbf{F}_i=-p\,\partial V/\partial\mathbf{r}_i$.

III. EMPTY ICOSAHEDRAL SHELLS

A word of caution concerning the T numbers of triangulated shells used by the authors of Refs. [13,14], and Caspar-Klug T numbers pertaining to viral shells is in order here. It should be understood that these two are not the same. For example, for the idealized virus structure in Fig. 1, the Caspar-Klug T number is 7 ($h=1$, $k=2$), while the T number characteristic of a kind of triangulation (without reference to pentamer/hexamer structures [13,14]) is 21 ($h=4$, $k=1$; this can be obtained by simply following a path from one pentamer to its neighboring pentamer with integer steps along the sides of the mesh triangles and not through the centers of the pentamer/hexamer structures). Of course, the two T numbers become the same if every vertex in the triangular mesh corresponds to the center of a capsomer. In what follows, I reserve the term "T number" for the characterization of the shell triangulation, while the term "Caspar-Klug T number" is used for the characterization of T numbers in the context in which they were originally introduced.

Icosahedral shells with various T numbers were constructed, and their total energy (E, which includes both stretching and bending contributions) as a function of bending modulus, κ was calculated. Other parameters of the Hamiltonian in Eq. (1) were been kept fixed ($a=1$, $\epsilon=1$). The initial shape for $\kappa\rightarrow\infty$ was set up [typically a sphere with a radius of $a\sqrt{5T\sqrt{3}/\pi}/2$, see Eq. (10)], and the minimum energy shape was obtained by an efficient implementation of the conjugate gradient method described in Ref. [20]. The resulting shape is used as an initial guess for the situation in which κ is decreased, and this procedure is repeated until κ becomes rather small. As demonstrated by the authors of Ref. [13], the shape and energy of continuous shells (large T numbers) are unique functions of the FvK number, which can be expressed as

$$\gamma = \langle R\rangle^2\frac{Y}{\kappa}, \quad (5)$$

where $\langle R\rangle$ is the mean radius of the shell given as

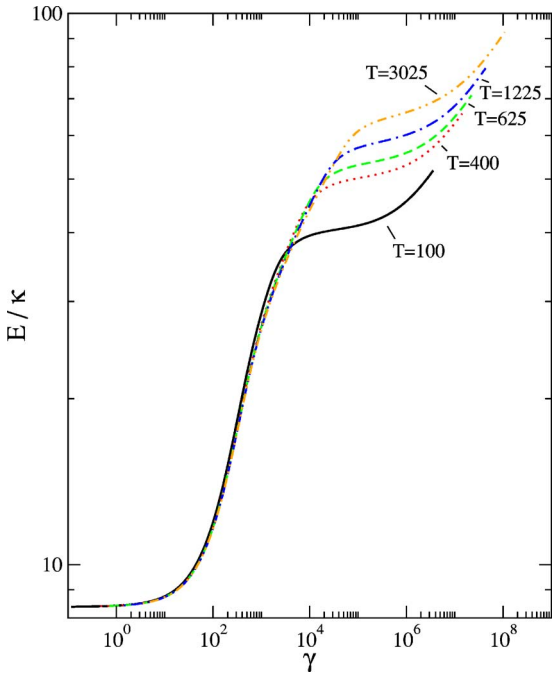

FIG. 2. (Color online) Shell energy as a function of the Föppl–von Kármán number for several T numbers as denoted in the figure ($T=100$, 400, 625, 1225, 3025).

$$\langle R\rangle = \frac{1}{N}\sum_{i=1}^{N} |\mathbf{r}_i - \mathbf{r}_0|, \tag{6}$$

and $\mathbf{r}_0$ is a geometrical center of the shape, $\mathbf{r}_0=\Sigma_{i=1}^{N}\mathbf{r}_i/N$. The total shell energy as a function of FvK number is shown in Fig. 2 for shells with different T numbers.

It can be seen that the continuum regime concerning the total energy of the shell is reached rather slowly and large T numbers are needed in this respect. This is especially true in the region of large FvK numbers ($\gamma>20\,000$). Shells with smaller T numbers can reliably predict the continuum shapes in the region $0<\gamma<20\,000$.

Based on quite general considerations, the authors of Ref. [13] concluded that the energy of a closed triangular shell (without the enclosed volume conservation constraint) with 12 pentagonal disclinations situated at the icosahedron vertices should behave as

$$\frac{E}{\kappa} = \begin{cases} 6B\gamma/\gamma_b + D, & \gamma < \gamma_b \\ 6B[1+\ln(\gamma/\gamma_b)] + D, & \gamma > \gamma_b, \end{cases} \tag{7}$$

where D is a constant contribution to the energy due to the background curvature of a sphere, B is a numerical constant which could be interpreted as a pentagonal disclination core energy and which should be reasonably close to $\pi/3$, and γ_b is a critical FvK number indicating approximately the region in which the buckling transition takes place. For the (unbuckled) shapes described by $\gamma<\gamma_b$, the total energy is approximately given by the sum of elastic stretching energy of 12 "unbuckled" pentagonal disclinations ($6B\gamma/\gamma_b$) and by the "background" elastic energy, D. There is no buckling contribution related to pentagonal disclinations other than the

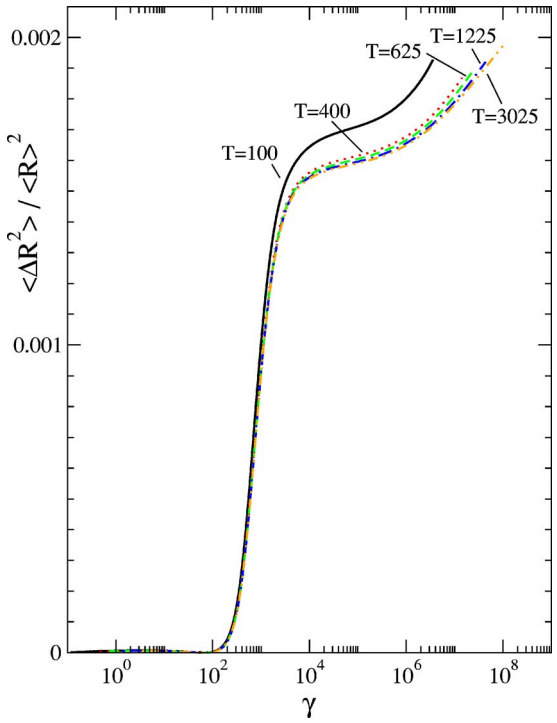

FIG. 3. (Color online) Mean square asphericity of minimal energy shapes as a function of the Foppl–von Kármán number for several T numbers as denoted in the figure ($T=100$, 400, 625, 1225, 3025).

overall, mean background curvature. For the buckled shapes ($\gamma>\gamma_b$), the functional dependence of the energy related to disclinations profoundly changes, and one has to account for the energies resulting from the bending of the conical section in the vicinity of each of the disclinations. This results in a logarithmic dependence of energy on γ. Further details can be found in Refs. [13–15]. The data for the largest T number ($T=3025$; $h=55$, $k=0$) were fitted to the analytical forms in Eq. (7), with B,D, and γ_b treated as fit parameters. I have found that the best fit to the numerical results in the region of $\gamma\in\langle 0,31\,000]$ is obtained with $B=1.29$, $\gamma_b=264$, and $D=8.51$. These numbers are in good agreement with the results reported in Ref. [14] ($B=1.27$, $\gamma_b=260$ [21]), but γ_b is two times larger from the value found in Ref. [13]. However, this value is not really "critical," since none of the characteristics of the shape undergo a discontinuous change at γ_b (see Fig. 3).

Mean square asphericities of shapes defined as in Ref. [13],

$$\frac{\langle \Delta R^2\rangle}{\langle R\rangle^2} = \frac{1}{N}\sum_{i=1}^{N}\frac{(|\mathbf{r}_i-\mathbf{r}_0|-\langle R\rangle)^2}{\langle R\rangle^2}, \tag{8}$$

are plotted in Fig. 3 as a function of γ for the same choice of T numbers as in Fig. 2.

The shape geometries apparently converge with the T number faster than the total energies (compare Fig. 2 and 3). Note that the buckling transition directly transcribes into increased mean square asphericities of the minimal energy shapes. The results are very similar to those presented in Ref. [13].

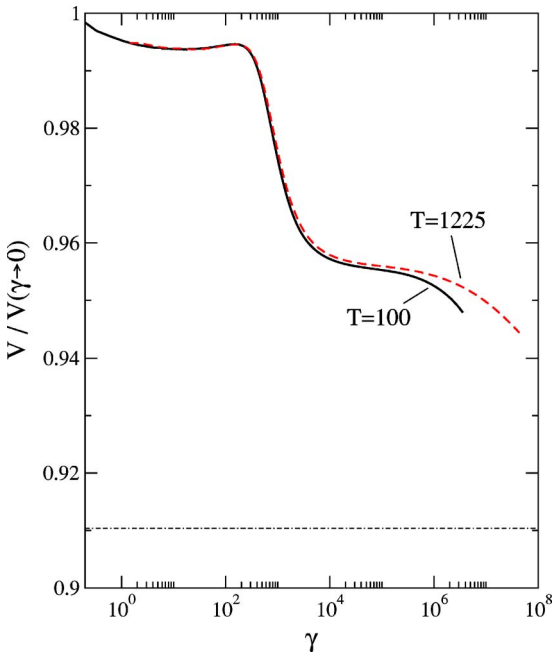

FIG. 4. (Color online) Volume enclosed by the shell as a function of the Föppl–von Kármán number for two values of the T number as denoted in the figure ($T=100$, 1225).

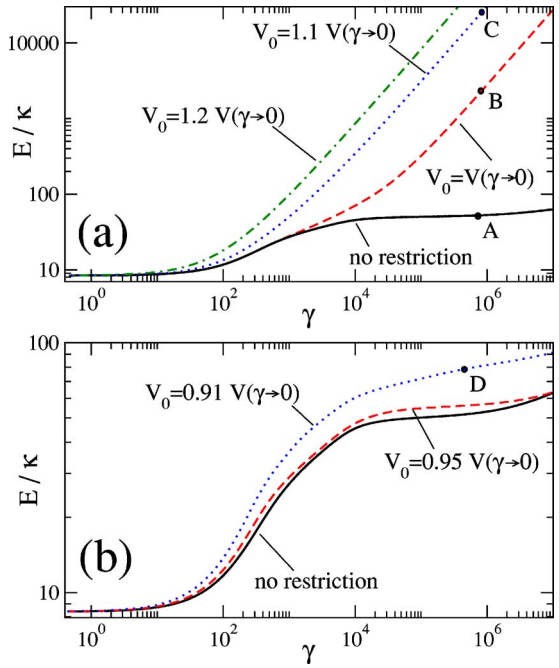

FIG. 5. (Color online) Comparison of shell energies with and without the volume conservation constraint as a function of the Föppl–von Kármán number for $T=400$. (a) Enclosed volumes are constrained to values larger than (or equal to) $V(\gamma\rightarrow 0)$; $V=V_0=V(\gamma\rightarrow 0)$, $V=V_0=1.1V(\gamma\rightarrow 0)$, and $V=V_0=1.2V(\gamma\rightarrow 0)$ as denoted in the figure. (b) Enclosed volumes are constrained to values smaller than $V(\gamma\rightarrow 0)$; $V=V_0=0.95V(\gamma\rightarrow 0)$ and $V=V_0=0.91V(\gamma\rightarrow 0)$ as denoted in the figure. The energy of unconstrained shells is also shown for comparison.

It is of interest to examine how the volume enclosed by the shell changes during the buckling transition. Rough estimates can be easily obtained. For small FvK numbers, the minimal energy shapes are very nearly spherical, while for extremely large FvK numbers, the shapes are nearly perfect icosahedra. Assuming that the shape area is the same in both limits, the volume ratio should be close to

$$\frac{V(\gamma\rightarrow\infty)}{V(\gamma\rightarrow 0)}\approx 0.91. \tag{9}$$

In fact, $V(\gamma\rightarrow 0)$ can be well approximated as

$$V(\gamma\rightarrow 0)\approx\frac{a^3}{6\sqrt{\pi}}(5T\sqrt{3})^{3/2}. \tag{10}$$

The above expression neglects the elastic strain in the spherical structure and assumes that all the triangular faces of the mesh have equal areas of $a^2\sqrt{3}/4$, which is, of course, untrue, especially in the regions close to pentagonal disclinations. Nevertheless, the numerically calculated value of $V(\gamma\rightarrow 0)$ was found to be only about 0.7 % smaller from the estimate in Eq. (10). Calculated changes of volume during buckling transitions are presented in Fig. 4. It can be seen that only about half of the maximum volume reduction predicted by Eq. (9) takes place during the buckling transition (for $100<\gamma<2000$), while the remaining part of the reduction takes place in the icosahedron's ridge-sharpening regime (for $\gamma>10^6$) studied in Refs. [22,23] and discussed also in Refs. [13,14].

IV. BUCKLING TRANSITION IN ICOSAHEDRAL SHELLS SUBJECTED TO THE FIXED ENCLOSED VOLUME CONSTRAINT

The model physical system that should be helpful in comprehending the results of this section is that of a formed shell with $\kappa\rightarrow\infty$, $\gamma\rightarrow 0$ (a sphere) into which an incompressible liquid is poured. The bending modulus of the shell is decreased and the change in energy and shape are monitored during the process. This picture is useful when the constrained volume is larger than the one in the limit $\kappa\rightarrow\infty$, $\gamma\rightarrow 0$, and the incompressible liquid is a rough approximation of the viral genetic material.

For the constrained shapes, FvK number is again calculated as in Eq. (5), although its meaning as the sole parameter that uniquely describes the shell shape [13] is obviously lost. The results of the calculation of shell energies with and without the enclosed volume constraint are presented in Fig. 5. Volumes V that are larger than $V(\gamma\rightarrow 0)$ seem to be of interest to the virus maturation process. To complete the picture of buckling transition in elastic shells (without respect to viruses), I have also considered the constraints to the total volume that are smaller than $V(\gamma\rightarrow 0)$.

The energies presented in Fig. 5 correspond only to the energy contained by the shell. For more realistic application of a shell theory to the viral shapes, one should also include the contribution of the capsid–DNA/RNA interaction in the

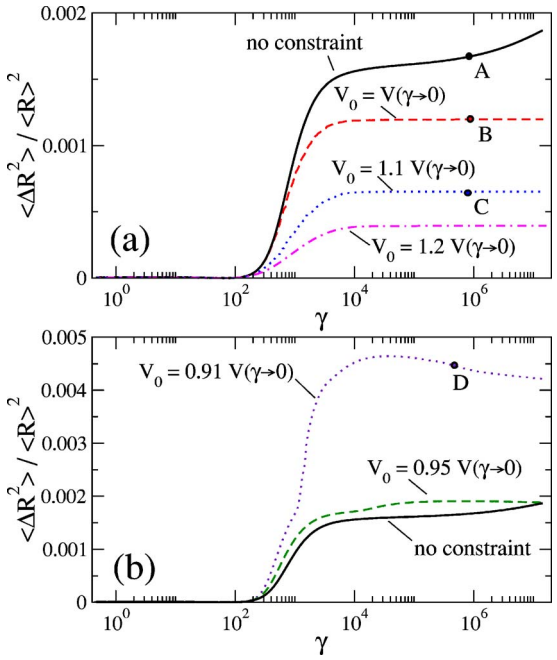

FIG. 6. (Color online) Mean square aspherity of unconstrained and constrained shells as a function of the Föppl–von Kármán number for $T=400$. The volume constraints studied are the same as in Fig. 5, and (a) and (b) display the results for constraints $V=V_0 \geq V(\gamma\rightarrow 0)$ and $V=V_0<V(\gamma\rightarrow 0)$, respectively.

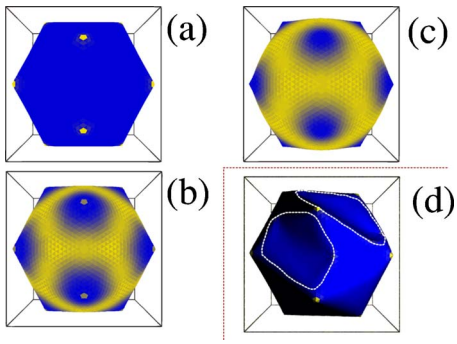

FIG. 7. (Color online) The buckled shapes for the Hamiltonian parameters denoted by A [(a) no volume constraint), B [(b) $V=V_0=V(\gamma\rightarrow 0)$], C [(c); $V=V_0=1.1V(\gamma\rightarrow 0)$] and D [(d); $V=V_0=0.91V(\gamma\rightarrow 0)$] in Figs. 5 and 6. The faces are colored according to their total energy. The brighter (yellow) triangles correspond to faces with large energy, while those of small total energy are darker (blue). Somewhat different lightning and shading of the shape was applied in (d), and the contrast was enhanced in order to emphasize the appearance of depressions in the shell, enclosed also by dotted lines.

total energy. It can be easily observed from Fig. 5(a) that the aspherical shell (viral) shapes become energetically very expensive for FvK numbers larger than about 10^4, and it is thus unlikely that shapes characterized by such large FvK numbers will be adopted by mature viral shells. This statement is corroborated by the fits of structures of bacteriophage HK97 and L-A yeast virus to the shapes predicted by Hamiltonian in Eq. (1), which produced values of $\gamma=1480$ and $\gamma=547$, respectively, [13] which are in the region of κ values where the volume conservation constraint does not increase the shell energy significantly (see Fig. 5). A critique of and limitations to this line of thinking and other possible explanations of the buckling transitions are presented in Sec. VI.

Note that the shell energies for volume constraints $V=V_0<V(\gamma\rightarrow 0)$ [Fig. 5(b)] do not increase significantly above those obtained without the volume constraint [compare energy scales in Fig. 5(a) and 5(b)]. Note that the volume constraint of $V=V_0=0.95V(\gamma\rightarrow 0)\approx V(\gamma=10^7)$ is *not* a constraint at the point when $\gamma\approx 10^7$, since at that point the volume adopted by the unconstrained shell equals the constrained volume (see Fig. 4). Thus, the energy curves for the unconstrained shape and the shape constrained to $V=V_0=0.95V(\gamma\rightarrow 0)$ touch at $\gamma\approx 10^7$.

Figure 6 displays how the mean square aspherity changes during the buckling transition for the constrained and unconstrained shapes. When the constrained volume is larger than $V(\gamma\rightarrow 0)$ [Fig. 6(a)], the final asphericities that are reached through the transition are notably lower in shapes with the fixed enclosed volume constraint, the more so the larger the fixed volume. The ridge-sharpening transition [22,23] seems to be suppressed, at least within the range of parameters studied here. When the constrained volume is smaller than $V(\gamma\rightarrow 0)$ [Fig. 6(b)], the shell shape changes more dramatically in the buckling transition, which can be seen by extremely large asphericities that are characteristic of shapes constrained to $V=V_0=0.91V(\gamma\rightarrow 0)$. The asphericities reached by these shapes cannot be explained by the flattening of the faces of the icosahedron, since the mean square aspherity of the perfect icosahedron is 0.002 598 3. A clue for such large asphericities can be found in Fig. 7 that shows buckled shapes for large FvK numbers. These shapes correspond to points denoted by A, B, C, and D in Figs. 5 and 6, i.e., they are calculated for the unconstrained case (A), in the case where volumes are constrained to $V=V_0=V(\gamma\rightarrow 0)$ (B), $V=V_0=1.1V(\gamma\rightarrow 0)$ (C), and $V=V_0=0.91V(\gamma\rightarrow 0)$ (D). The triangular faces in the shapes are colored according to the total energy that they contain. This was calculated as one half of the energy contained in the three edges of a particular triangle. Note how the distribution of energy contained in the shell changes depending on whether the enclosed volume conservation constraint is imposed or not. For unconstrained shells, the largest energy is contained in the vicinity of the pentagonal disclinations (similar effect was observed in Ref. [25]), while the *opposite* is observed for the shapes in which the constrained volume is larger than $V(\gamma\rightarrow 0)$. In that case the largest energy is contained in the regions *between* the disclinations that "bulge out" to satisfy the volume conservation constraint [Fig. 7(c)]. Practically all of this energy is of the stretching type, since the distances between the points on the shell (vertices) have to be larger from their equilibrium values in order to satisfy the constraint. This may have some implications to bursting of viral capsids, in particular, the points at which the cracks in the capsid initiate [25]. Particularly interesting is the shape obtained for $V=V_0=0.91V(\gamma\rightarrow 0)$ [Fig. 7(d)]. Some shading is applied in the depiction of this shape [unlike in shapes displayed in Figs. 7(a)–7(c)] in order to clearly emphasize its main characteristic—a *depression*, collapse, or *crumpling* of the

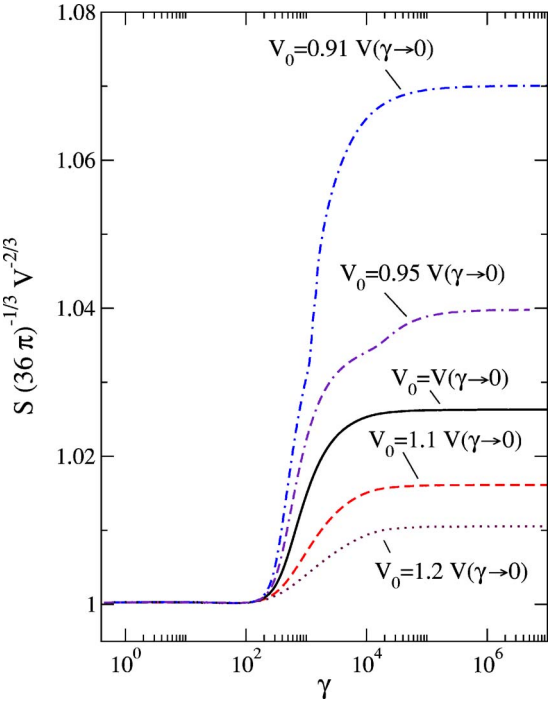

FIG. 8. (Color online) The normalized area of shells with constrained volumes as denoted in the figure as a function of the Föppl–von Kármán number (T=400).

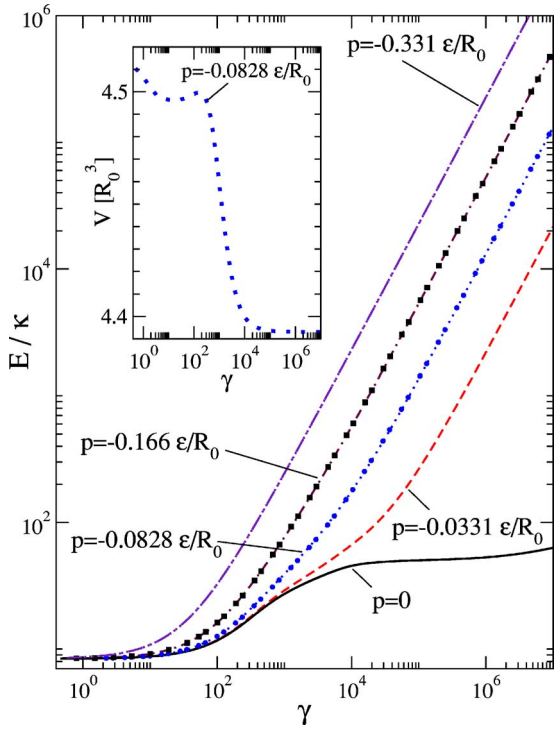

FIG. 9. (Color online) The shell energy as a function of the Föppl–von Kármán number for five different values of pressure, as denoted in the figure, that is acting on the shell from its inside. The calculations represented by the lines were performed for T=400 shells, and squares and circles represent the results of the calculation for T=625 and T=1225 shells, respectively. The shell energies without applied pressure (p=0) are shown for comparison. The inset displays the change in volume (measured in R_0^3 units, see text) of the T=400 shell subjected to the internal pressure of p=−0.0828ϵ/R_0 as a function of the Föppl–von Kármán number.

shell localized in between the disclinations. This is the reason for the extremely large asphericities observed in Fig. 6(b). Note that the highest energies in this case are localized in vicinity of the pentagonal disclinations, since the shell collapse does not require a large change in the stretching energy.

The total area (S) of the shapes also increases during the buckling transition under the constraint of fixed volume. The normalized area, $S(36\pi)^{-1/3}V^{-2/3}$ as a function of the FvK number is shown in Fig. 8. Note that for a perfect sphere, the normalized area as defined here is 1, and for icosahedron, it is 1.0646.

V. BUCKLING TRANSITION IN ICOSAHEDRAL SHELLS WITH THE CONSTANT INTERNAL PRESSURE

Before studying the effects of pressure on the icosahedral shells, it should be decided in what effective units the pressure is to be measured. The quantity that was kept fixed in the calculations presented thus far was ϵ, that is, the scale of energy related to stretching. The internal pressure necessarily induced stretching of the shell, and thus, the pressure should be expressed in units of ϵ divided by some spatial scale. It seems reasonable to chose the radius of the shell in the limit when $\kappa\to\infty, \gamma\to 0$, and p=0 as the relevant spatial scale. The radius of the shell in this limit is denoted as R_0, and the pressure is thus measured in the units of ϵ/R_0. I demonstrate that in the continuum limit of shells this indeed produces appropriate results which coincide for the shells of different (but still large) T numbers.

The effects of pressure that acts from the inside of the shell (negative pressures) on the shell energy is shown in Fig. 9. This can also be thought of as a situation in which the internal pressure in the shell is larger from the surrounding pressure. The quantity shown on the ordinate axis of Fig. 9 is the shell energy, that is the value obtained when pV is subtracted from the total Hamiltonian [see Eq. (4)]. Similar trends are observed here as in Fig. 5(a). For large internal pressures, the shell energies increase significantly above the values that are obtained when there is no pressure acting on the shell. The lines in the figure were calculated for T=400 shells. The radius of this shell in the limit when $\kappa\to\infty, \gamma\to 0$ is R_0=16.5682a [see Eq. (1)], so the pressures shown in Fig. 9 can also be expressed as $-0.002\epsilon/a$ $(-0.0331\epsilon/R_0)$, $-0.005\epsilon/a$ $(-0.0828\epsilon/R_0)$, $-0.01\epsilon/a(-0.166\epsilon/R_0)$, and $-0.02\epsilon/a$ $(-0.331\epsilon/R_0)$. The circles in Fig. 9 represent the results obtained for the T=625 shell with the applied pressure $p=-0.008003\epsilon/a$ $=-0.166\epsilon/R_0$, since R_0=20.7035a for the T=625 shell. Note that these results coincide with those obtained for the T=400 shell, which confirms both that the continuum limit is reached and the appropriateness of the units chosen for pressure. The same holds for the T=1225 shell [the squares in Fig. 9], for which R_0=28.9738a. When the constant internal pressure is applied to the shell, as the FvK number changes, so does the volume enclosed by the shell. The inset in Fig. 9

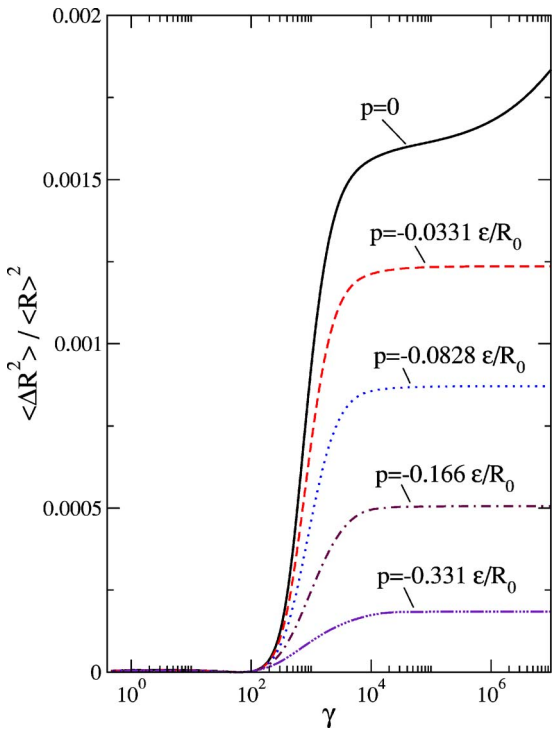

FIG. 10. (Color online) Mean square asphericities of the shells subjected to constant internal pressures, as denoted in the graph, as a function of the Föppl–von Kármán number ($T=400$).

displays the change of the enclosed volume (measured in R_0^3 units) with the FvK number for $p=-0.0828\epsilon/R_0$ ($T=400$). Note that the enclosed volume in the limit $\kappa\to\infty, \gamma\to 0$ is *not* $4\pi/3\approx 4.189$ but larger (about 4.6), which is simply because the effective internal force (pressure) acts on the shell and increases its volume. For all the pressures studied, the volume of the buckled shapes (in the limit when $\gamma\to\infty$) is smaller from the volume of unbuckled shapes (in the limit when $\gamma\ll\gamma_b$), and the difference between the two values of the volume becomes smaller with the increase (in absolute value) of the internal pressure. Note that the internal pressure necessarily induces the increase of the stretching energy of the shell. The effects of positive (outside) pressure on the shell energies and shapes could not be studied with the method presented in Sec. II B, since for some critical value of the FvK number, depending on the magnitude of the applied pressure, the shell abruptly collapses, crumples, and the numerical method chosen becomes unreliable for tracing this effect.

Mean square asphericities of the shapes are shown in Fig. 10. It is clear that large internal pressures suppress the change in asphericity in the buckling transition, but the transition is still observed within the region of pressures studied here. Note that this is not a trivial finding since for $p=-0.331\epsilon/R_0$, the enclosed shell volume for $\gamma=0.6$ is 1.4 times larger from the volume that would be enclosed by the shell without the applied pressure, yet the buckling transition still survives.

VI. APPLICATION OF THE RESULTS TO VIRAL SHAPES

It is of use to scale the pressures studied in Sec. V to circumstances that are relevant to viruses. To do this, an estimate of the elastic parameters of the viral coatings is needed. The authors of Ref. [13] have suggested that the ratio Y/κ appropriate for viruses is about 1–2 nm^{-2}. The authors of Ref. [14] have taken a step further and they estimate that the Young's modulus of the viral coating is about $Y=10k_BT/\mathrm{nm}^2$. The scale of the stretching energy ϵ is of the same order of magnitude as Y [see Eq. (1) and the discussion following it]; thus, I fix ϵ to $10k_BT/\mathrm{nm}^2$. The radius of the virus in its spherical (immature) form depends on the virus in question. If one considers HK97 bacteriophage procapsid of radius $R_0=26$ nm, the scale of pressure for this virus is $\epsilon/R_0=0.2k_BT/\mathrm{nm}^3=1\,657\,000$ Pa$\approx$16.4 atm. The highest pressure studied ($-0.331\epsilon/R_0$) would thus, in the case of HK97 bacteriophage, be about 548 600 Pa$\approx$5.42 atm. It is of interest to compare these numbers to those obtained in Ref. [26]. In studying the energetics of DNA inserted in the preformed viral capsids, the authors have found [26] that for a virus of radius 27.5 nm, the pressure that the fully packed DNA genome (whose length is 16.5 μm) exerts on its walls is about 30–45 atm. For a virus of such radius, the pressure scale introduced in this article should be about $\epsilon/R_0\approx 15.5$ atm, assuming the same value for ϵ as for the HK97 bacteriophage. The highest pressure studied in this work would then correspond to 5.1 atm, about six times smaller from the pressure acting in the filled viral capsid of the virus studied in Ref. [26]. Similar estimate for the pressure that the fully loaded genetic material exerts on the viral coating was obtained in Ref. [27]. For $\phi 29$ bacteriophage, the authors estimate that the internal pressure is about 60 atm, in agreement with previous estimates from Ref. [28]. There is an obvious agreement in the literature concerning the internal pressures in mature viral capsids. However, for such large internal pressures, and assuming that $\epsilon=10k_BT/\mathrm{nm}^2$, the mean square asphericities of buckled shapes (i.e., mature viruses) should be very small (see Fig. 10), far smaller than observed, e.g., for mature HK97 capsid (0.00116). On the other hand, one could insist on the application of the present model to viruses and use the results presented here to reestimate the value of the Young's modulus of the coating of a mature virus. In other words, the aim is to scale the internal pressures to the values obtained in previous studies and to obtain new estimates for elastic parameters of mature viral capsid. I again concentrate on the HK97 virus. Assuming that the capsid's elastic parameters are in the region where the mean square asphericity saturates, the internal pressure should be about $0.045\epsilon/R_0$ (see Fig. 10; this internal pressure results in final asphericity that is about the same as in mature HK97 virus). Equating this with the estimated internal pressure of about 40 atm [29] and using $R_0=26$ nm, one obtains that for the mature HK97 virus, $Y\approx 650k_BT/\mathrm{nm}^2$ (2.7 N/m), about 60 times larger from the estimate of Ref. [14], but closer to the alternative (discarded) estimate of Ref. [14], which was about $Y\approx 1$ N/m. The bending rigidity should then be smaller than about 1.8×10^{-19} J ($\gamma>10^4$, see Fig. 10). Division of the two-dimensional Young's modulus obtained in this study with the thickness of the mature HK97 viral shell (about 2.5 nm [17,18]) yields an approximate prediction for the 3D (bulk) Young's modulus (Y_{3D}) of the viral protein shell. This procedure gives $Y_{3D}=1.1$ GPa, which is about 40 % smaller from the value found in the experimental study

of the elastic response of empty viral shells of $\phi 29$ bacteriophage with the use of atomic force microscopy (AFM) (1.8 GPa) [30]. Note, however, that the results obtained here relate to elastic properties of *mature* (filled) viral shells, while the experimental results are performed on empty capsids. Nevertheless, the results obtained here suggest that the Young's modulus of the viral coating may be significantly larger than predicted in Ref. [14] and closer to the value discarded by authors of that work. The alternative value of Young's modulus was discarded by authors of Ref. [14] on the basis of Monte Carlo simulations of a coarse-grained capsomer [3] model which yielded that the bending rigidity κ should be of the order of the capsomer-capsomer cohesive binding energy. Thus, the results presented here may point toward improvements in the coarse-grained model of viruses.

Pouring a liquid into a spherical elastic shell (immature capsid), or applying a pressure to it from the inside will not, of course, change its shape to a more aspherical one. What ought to happen "during pouring" (the insertion of a genetic material) is a dynamical process that changes the elastic properties of a capsid, i.e., that effectively increases its FvK number. Only then will a mature capsid be more aspherical than the precursor capsid. Thus, the results presented in this article cannot provide the full physical description of virus maturation. Nevertheless, if the change of the capsid shape is influenced by the fact that the capsid is filled with the genetic material (in the most trivial sense of finite volume occupation or simulated by the constant internal pressure), the results should prove useful. The presented results essentially show that if there is a process that increases the effective FvK number of the capsid, the volume conservation constraint or finite internal pressure that may be imposed by the inserted genetic material is not strong enough to destroy the signatures of the buckling transition, and the mature shell will be more aspherical from its precursor shell, although to lesser amount than could be concluded from the study of buckling transition in empty shells (see Fig. 6). Now, what could be the process that induces the change of elastic properties of the viral capsid?

The proposition put forth by Lidmar *et al.* [13] is that the FvK number changes during the maturation due to the increase of radius (R) and decrease of effective thickness of the protein coating, d. According to Ref. [13], if one approximates a shell by a uniform isotropic elastic medium of thickness d with the Poisson ratio ν_3, then its effective FvK number should be about

$$\gamma = 12(1 - \nu_3^2)(R/d)^2. \tag{11}$$

If one additionally assumes that the volume of the capsid protein material (not the volume *enclosed* by the capsid) remains the same and that ν_3 does not change during maturation, then the FvK numbers before (γ_B) and after (γ_A) the transition for the HK97 capsid studied in Ref. [13] should be $\gamma_B \approx 630$ and $\gamma_A = 1480$. This predicts a noticeably more spherical shape of the immature capsid. It has been experimentally observed that the capsid proteins rearrange themselves significantly during maturation [24]. To a lesser extent, the reorganization involves the refolding of the protein

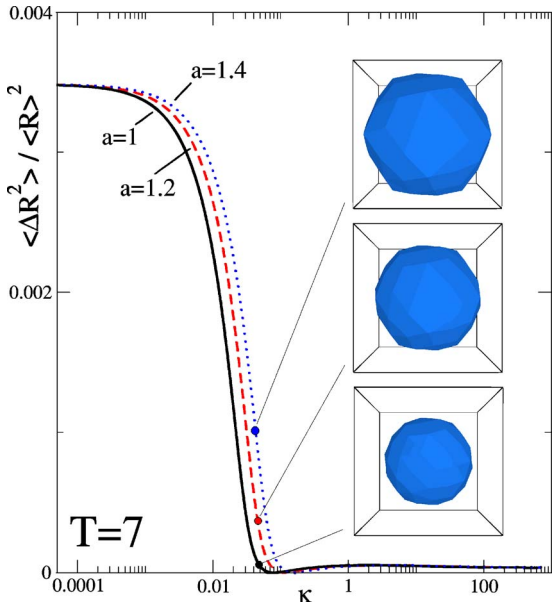

FIG. 11. (Color online) Mean square asphericities of $T=7$ shells as a function of bending modulus. The calculations for three different values of the lattice constant a are displayed ($a=1.0$, full line; $a=1.2$, dashed line; and $a=1.4$, dotted line). The three shapes characterized by these three lattice constants are plotted for $\kappa=0.0458$.

itself, but its main consequence is a rearrangement (translations and rotations) of the proteins to another configuration in which the contacts between capsomers change and the capsomers adopt a more symmetrical shape, which also results in a smoother shape of the capsid. This rearrangement has been studied in detail for bacteriophage HK97 and P22 capsid in Refs. [17,18], respectively. These experimental findings suggest that one should study the effects of a change of the lattice constant, a, on the shape of the minimum energy shells. This was done in Fig. 11. The calculations were intentionally performed for small value of T number ($T=7$, which corresponds to the symmetry of HK97 capsid), although one should keep in mind that the Hamiltonian in Eq. (1) was constructed with the idea of treating the continuous (large T number) structures for which it makes sense to speak about elastic parameters of protein sheets, and its predictions for small T numbers should not be directly transcribed to viral shapes. Nevertheless, the form in which the Hamiltonian is written [Eq. (1)] suggests its "microscopic" interpretation. These subtleties were discussed in Refs. [13,14]. The calculations in Fig. 11 were performed for three values of the lattice constant, $a=1$, $a=1.2$, and $a=1.4$. The scale of the elastic energy was kept constant ($\epsilon=1$), and the bending modulus κ was changed. The mean square asphericities were plotted as a function of κ. The constraint of fixed enclosed volume was not implemented and $p=0$. Note that in the critical region of values of κ (onset of the buckling transition), the shapes with very different asphericities can be produced by simply changing the lattice parameter a and keeping all other parameters of the Hamiltonian fixed (for the shapes plotted in Fig. 11, the bending modulus was $\kappa = 0.0458$). This numerical experiment reproduces the experimental findings that the (i) mature viral shapes enclose larger

volume, and (ii) mature viral shapes are more facetted from their precursor shapes. Of course, it still does not provide any clues with respect to the process that drives the transition to larger lattice constant.

VII. SUMMARY AND CONCLUSIONS

The buckling transition of shells with 12 pentagonal disclinations situated in vertices of an icosahedron was studied. The constraint of the fixed enclosed volume was introduced and its effect on the shell shapes and energies explored. The shell shapes and buckling transition were also investigated in cases when the constant internal pressure acts on the shell. It was found that the buckling transition survives the volume constraint, at least for the enclosed volumes that are not too large. The buckled shapes are found to be less aspherical than the ones obtained without the volume constraint. Similar conclusions were reached for shells subjected to constant internal pressure. For pressures that are not too large (about $p=-0.3\epsilon/R_0$), the buckling transition survives and the buckled shapes are significantly more aspherical from the ones in the region of small FvK numbers. If one transcribes the results of the study of shells under constant internal pressures to the circumstances appropriate to viruses [27,28], an estimate of the two-dimensional Young's modulus of the coating can be obtained, and for mature HK97 virus, the value of $Y\approx 2.7$ N/m was found. This also puts an upper limit on bending rigidity, $\kappa\leq 1.8\times 10^{-19}$ J. For the bulk (3D) Young's modulus of the viral coating material, this yields a value of about $Y_{3D}\approx 1.1$ GPa, which is close to the value found in experimental studies of elastic response of empty $\phi 29$ bacteriophage shells [30].

Whether the fixed enclosed volume of the shell, or the constant internal pressure is a realistic model of the (mature) viral shells filled with the genetic material is, of course, questionable, and alternative scenarios for the virus maturation, based again on the triangulated elastic shells, have been proposed in Sec. VI. In any case, the results of this article should be of use in extending the approaches of Refs. [13,14] toward more realistic modeling of viral shapes.

[1] H. Fraenkel-Conrat and B. Singer, Philos. Trans. R. Soc. London, Ser. B **354**, 583 (1999).
[2] R. F. Bruinsma, W. M. Gelbart, D. Reguera, J. Rudnick, and R. Zandi, Phys. Rev. Lett. **90**, 248101 (2003).
[3] R. Zandi, D. Reguerra, R. F. Bruinsma, W. M. Gelbart, and J. Rudnick, Proc. Natl. Acad. Sci. U.S.A. **101**, 15556 (2004).
[4] R. Twarock, J. Theor. Biol. **226**, 477 (2004).
[5] D. L. D. Caspar and E. Fontano, Proc. Natl. Acad. Sci. U.S.A. **93**, 14271 (1996).
[6] Notable exceptions are polyoma and the closely related Simian virus 40 (SV-40) which contain 72 pentamers and no hexamers; see, e.g., L. Makowski, Biophys. J. **74**, 534 (1998).
[7] H. W. Kroto and K. McKay, Nature (London) **331**, 328 (1988).
[8] G. J. Morgan, TIBS **28**, 86 (1993).
[9] V. Reddy, P. Natarajan, B. Okerberg, K. Li, K. Damodaran, R. Morton, C. Brooks, III, and J. Johnson, J. Virol. **75**, 11943 (2001); see also Viper Particle Explorer webpage athttp://viperdb.scripps.edu
[10] H. Kroto, Rev. Mod. Phys. **69**, 703 (1997).
[11] A. Šiber, Phys. Rev. B **70**, 075407 (2004).
[12] D. L. D. Caspar and A. Klug, Cold Spring Harbor Symp. Quant. Biol. **27**, 1 (1962).
[13] J. Lidmar, L. Mirny, and D. R. Nelson, Phys. Rev. E **68**, 051910 (2003).
[14] T. T. Nguyen, R. F. Bruinsma, and W. M. Gelbart, Phys. Rev. E **72**, 051923 (2005).
[15] H. S. Seung and D. R. Nelson, Phys. Rev. A **38**, 1005 (1988).
[16] T. S. Baker, N. H. Olson, and S. D. Fuller, Microbiol. Mol. Biol. Rev. **63**, 862 (1999).
[17] J. F. Conway, W. R. Wikoff, N. Cheng, R. L. Duda, R. W. Hendrix, J. E. Johnson, and A. C. Steven, Science **292**, 744 (2001).
[18] W. Jiang, Z. Li, Z. Zhang, M. L. Baker, P. E. Prevelige, Jr., and W. Chiu, Nat. Struct. Biol. **10**, 131 (2003).
[19] J. Nocedal and S. J. Wright, *Numerical Optimization* (Springer-Verlag, New York, 1999).
[20] W. W. Hager and H. Zhang, SIAM J. Optim. **16**, 170 (2005).
[21] I use the definition of Föppl–von Kármán number from Ref. [13] which differs from the one in Ref. [14] by a multiplicative factor of $(4\pi)^{-1}$.
[22] A. E. Lobkovsky, Phys. Rev. E **53**, 3750 (1996).
[23] A. E. Lobkovsky and T. A. Witten, Phys. Rev. E **55**, 1577 (1997).
[24] A. C. Steven, B. L. Trus, F. P. Booy, N. Cheng, A. Zlotnick, J. R. Caston, and J. F. Conway, FASEB J. **11**, 733 (1997).
[25] R. Zandi and D. Reguera, Phys. Rev. E **72**, 021917 (2005).
[26] S. Tzlil, J. T. Kindt, W. M. Gelbart, and A. Ben-Shaul, Biophys. J. **84**, 1616 (2003).
[27] P. K. Purohit, J. Kondev, and R. Phillips, Proc. Natl. Acad. Sci. U.S.A. **100**, 3173 (2003).
[28] D. E. Smith, S. J. Tans, S. B. Smith, S. Grimes, D. L. Anderson, and C. Bustamante, Nature (London) **413**, 748 (2001).
[29] P. K. Purohit, M. M. Inamdar, P. D. Grayson, T. M. Squires, J. Kondev, and R. Phillips, Biophys. J. **88**, 851 (2005).
[30] I. L. Ivanovska, P. J. de Pablo, B. Ibarra, G. Sgalari, F. C. MacKintosh, J. L. Carrascosa, C. F. Schmidt, and G. J. L. Wuite, Proc. Natl. Acad. Sci. U.S.A. **101**, 7600 (2004).